Brain Pathology

**RESEARCH ARTICLE**

# Distinct Aβ pathology in the olfactory bulb and olfactory deficits in a mouse model of Aβ and α-syn co-pathology

Marina Friesen[1,2,3] | Stephanie Ziegler-Waldkirch[1,2] | Milena Egenolf[1,2] |
Paolo d'Errico[1,2] | Christina Helm[1,2] | Charlotte Mezö[2,3,4] | Nikolaos Dokalis[2,3,4] |
Daniel Erny[2,4,5] | Natalie Katzmarski[1,2] | Romina Coelho[1,2,6] | Desirée Loreth[1,2,7] |
Marco Prinz[2,4,8,9] | Melanie Meyer-Luehmann[1,2,8]

[1]Department of Neurology, Medical Center, University of Freiburg, Freiburg, Germany

[2]Faculty of Medicine, University of Freiburg, Freiburg, Germany

[3]Faculty of Biology, University of Freiburg, Freiburg, Germany

[4]Institute of Neuropathology, University of Freiburg, Freiburg, Germany

[5]Berta-Ottenstein-Programme, Faculty of Medicine, University of Freiburg, Freiburg, Germany

[6]Biosystems and Integrative Sciences Institute, Faculdade de Ciências, Departamento de Química e Bioquímica, Universidade de Lisboa, Lisbon, Portugal

[7]Institute of Cellular and Integrative Physiology, University Medical Center Hamburg-Eppendorf, Hamburg, Germany

[8]Center for Basics in NeuroModulation (NeuroModulBasics), Faculty of Medicine, University of Freiburg, Freiburg, Germany

[9]Signalling Research Centres BIOSS and CIBSS, University of Freiburg, Freiburg, Germany

**Correspondence**
Melanie Meyer-Luehmann, Department of Neurology, Neurocenter, Breisacherstr. 64, Freiburg 79106, Germany.
Email: melanie.meyer-luehmann@uniklinik-freiburg.de

## Abstract

Several degenerative brain disorders such as Alzheimer's disease (AD), Parkinson's disease (PD) and Dementia with Lewy bodies (DLB) are characterized by the simultaneous appearance of amyloid-β (Aβ) and α-synuclein (α-syn) pathologies and symptoms that are similar, making it difficult to differentiate between these diseases. Until now, an accurate diagnosis can only be made by *postmortem* analysis. Furthermore, the role of α-syn in Aβ aggregation and the arising characteristic olfactory impairments observed during the progression of these diseases is still not well understood. Therefore, we assessed Aβ load in olfactory bulbs of APP-transgenic mice expressing $APP695^{KM670/671NL}$ and $PSEN1^{L166P}$ under the control of the neuron-specific *Thy-1* promoter (referred to here as *APPPS1*) and *APPPS1* mice co-expressing $SNCA^{A30P}$ (referred to here as *APPPS1 × [A30P]aSYN*). Furthermore, the olfactory capacity of these mice was evaluated in the buried food and olfactory avoidance test. Our results demonstrate an age-dependent increase in Aβ load in the olfactory bulb of APP-transgenic mice that go along with exacerbated olfactory performance. Our study provides clear evidence that the presence of α-syn significantly diminished the endogenous and seed-induced Aβ deposits and significantly ameliorated olfactory dysfunction in *APPPS1 × [A30P]aSYN* mice.

**KEYWORDS**
Alzheimer's disease, amyloid-β plaques, Aβ seeding, dementia with Lewy bodies, olfaction, olfactory bulb, α-synuclein

---

Marina Friesen and Stephanie Ziegler-Waldkirch are contributed equally to this work.

------------------

# 1 | BACKGROUND

Dementia with Lewy bodies (DLB) is the second most common type of dementia that involves the deposition of amyloid-β (Aβ) plaques and α-synuclein (α-syn)-containing Lewy bodies as pathological hallmarks of Alzheimer's disease (AD) and Parkinson's disease (PD), respectively [1–5]. Despite being initially described as two separate neurodegenerative disorders, several independent studies confirmed that clinical symptoms and pathologies of AD and PD can overlap [6, 7]. Interestingly, up to 50% of all AD cases display co-occurrence of α-syn in histopathological brain examinations [8–10] and about 40% of PD patients exhibit additionally Aβ pathology [11, 12]. Consequently, it was previously verified that these proteins can directly interact and form complexes when isolated from human or mouse brains harbouring both pathologies [13–17]. As the identification of DLB in the context of dementia with an AD pattern is however still difficult and often leads to a misdiagnosis of AD or PD, biomarkers are necessary to improve identification of disease subtypes underlying dementia [18, 19].

A common feature of neurodegenerative diseases is the occurrence of olfactory dysfunctions at a very early stage of disease progression, even years before other clinical symptoms occur [20, 21]. While major progress has been made to decipher the role of the olfactory bulb for AD and PD, little is known about its impact on DLB. Therefore, studies of early pathological alterations in the olfactory bulb are of great interest in order to use olfactory deficits as a biomarker for early diagnoses and disease progression. The olfactory bulb is the entry site for the processing of odours and involves different types of cells such as mitral and granule cells that are essential for the processing of olfactory information.

Several studies implied a correlation between olfactory impairment and Aβ burden in mice [22–24]. Interestingly, individuals as well as mice with additional α-syn pathology appeared to have lowered Aβ pathology [25, 26]. In the present study, we therefore examined the effect of α-syn on the formation of Aβ aggregates specifically in the olfactory bulb and the potential arising impact on olfactory performance in a mouse model of Aβ and α-syn co-pathology. Here, we show that α-syn diminished the Aβ load in the olfactory bulb of these mice and that overlap of both pathologies led to a significant amelioration of olfactory performance.

# 2 | MATERIALS AND METHODS

## 2.1 | Animals

All animal experiments were carried out in accordance with the policies of the state of Baden-Württemberg under license number G16-100, G18-136.

We used heterozygous *APPPS1* transgenic mice co-expressing human $APP695^{KM670/671NL}$ and $PSEN1^{L166P}$ under the control of the neuron-specific *Thy-1* promoter [27] and heterozygous $Thy-1-SNCA^{A30P}$ transgenic mice [28], referred to as *aSYN* mice. *APPPS1* mice were crossed to heterozygous *aSYN* mice to generate *APPPS1 × [A30P]aSYN* double transgenic mice [22]. We used *APPPS1*, *APPPS1 × [A30P]aSYN* and non-transgenic littermates (wild-type, WT). All mice were on the C57BL/6 background. For the present study, male mice were used as indicated in the text unless stated otherwise. Mice were used at the age of 4, 8 and 12 months. Animals were group-housed under specific pathogen-free conditions. All mice were kept under a 12-h light, 12-h dark cycle with food and water *ad libitum*.

The precise number of mice used and analysed are displayed in Tables S1 and S2.

## 2.2 | Olfaction test

For olfaction tests, 4- and 8-month-old male *APPPS1*, *APPPS1 × [A30P]aSYN* and WT mice were used. All experiments were done in the morning.

## 2.3 | Buried food test

The buried food (cookie) test is based on the time it took a mouse to find a hidden buried cookie in the bedding, as described previously [29]. In brief, mice were exposed to the cookie for 2 days before the test. The day after, mice were fasted 12 h before the test and habituated to the testing room for 1 h. The test began by placing the mouse in a clean cage (41 cm length × 26 cm width × 18 cm height) containing 3 cm deep bedding. Following 10 min of habituation, a cookie was placed 0.5 cm below the bedding. The latency to find the cookie was measured. The mouse was considered to have uncovered the cookie when it started to eat the cookie. If the mouse did not find the cookie within 15 min, the test was ended and the mouse was excluded from the experiment.

## 2.4 | Olfactory avoidance test

An olfactory avoidance test was performed as described previously [30]. Mice were habituated to the testing room for at least 1 h. The test started by placing the mouse in a clean cage (33 cm length × 20 cm width × 12.5 cm height) containing 3 cm deep bedding. The test cage was divided optically into two equal areas. After 10 min of habituation to the test cage, a cotton swab scented with nTMT (2,4,5-Trimethylthiazole, Sigma–Aldrich, 1:100 diluted in water) was placed in one half of the test cage. Avoidance time was measured during a 60 s test time. 'Avoidance time' was defined as the time spent in the area without a

cotton swab scented with nTMT. Avoidance behaviour was represented by an avoidance index as follows: avoidance index = $(P - 50)/50$, where $P$ is the percentage of avoidance time during a 60 s test period.

## 2.5 | Histology

Mice were transcardially perfused with 10 ml of ice-cold phosphate-buffered saline (1×PBS) followed by 10 ml of ice-cold 4% paraformaldehyde in PBS. Brains were isolated and post-fixed in 4% PFA (Roti®-Histofix, Roth) for 24 h, followed by incubation in 30% sucrose (in 1XPBS, pH 7.5) for further 48 h. Frozen brains were cut into 25-µm-thick coronal sections on a sliding microtome (SM2000R, Leica Biosystems, Wetzlar, Germany) and collected in 15% Glycerol. Sections were incubated overnight at 4°C with the following antibodies diluted in 1XPBS containing 5% normal goat serum (NGS) and 0.5% Triton X-100: anti-Aβ (mouse, 1:2000, Covance, 6E10), anti-Iba1 (rabbit, 1:1000 WAKO, 019–19741), anti-CD68 (rat, 1:500, BioRad, FA-11), anti-Lamp2 (rat, 1:500, Abcam, ab13524), anti-Reelin (mouse, 1:1000, Merck Millipore, MAB5364). Appropriate secondary antibodies conjugated to Alexa 488 (Life Technologies A11029, A11008), Alexa 555/568 (Life Technologies A21422, A11011) or Alexa 647 (Life Technologies A21235) (1:1000) were used. Sections were counterstained with DAPI (Sigma, D9542, 1:10000) and mounted with fluorescence mounting medium (DAKO).

NeuroTrace 500/525 (green fluorescent Nissl stain, N21480, Thermo Fisher Scientific) staining was done according to manufactural instructions.

Dense-core plaques were stained with Thiazine red (Sigma Aldrich, S570435). Staining was done according to standard protocols. In brief, sections were washed three times in 1×PBS and incubated in Thiazine red (0.01% solution in 1XPBS) for 5 min at RT followed by 3 × 10 min washes in 1×PBS. Sections were counterstained with DAPI (Sigma, D9542, 1:10000) and mounted with fluorescence mounting medium (DAKO, S3023).

## 2.6 | Assessment of Aβ and cell analysis

Fluorescence images of brain slices were taken using a Zeiss fluorescent microscope (Axio Imager M2M). Confocal images were taken with an Olympus confocal microscope (Fluoview FV 1000). For analysis every 10th brain section was immunostained. The area of the olfactory bulb and the mitral cell layer was defined based on the mouse brain atlas [31]. The 25-µm-thick serial coronal sections represented always the same layers in each animal, starting from Bregma 5.0 to Bregma 3.7.

Total Aβ load was determined by calculating the % areal fraction occupied by Aβ-positive staining in the olfactory bulb using the imaging software ImageJ

(National Institutes of Health freeware, version 1.52a). Five to eight animals per group and 4–5 sections per animal were analysed.

Cell number was quantified by counting the number of positive-labelled cells in the area of interest of the animals. Five animals per group and 4–5 sections per animal were analysed. Cell counting was done in the olfactory bulb and the area of the olfactory bulb was measured with the ImageJ software (version 1.52a). Cell counts were performed within a defined volume based on the region of interest and the thickness of the section (25 µm). All analyses were conducted in a blinded manner.

## 2.7 | Immunoblot analysis of the olfactory bulb

Mouse olfactory bulb tissue was dissected on ice and homogenized in 10× volume RIPA buffer [50 mM HEPES pH 7.5, 150 mM NaCl, 1 mM EDTA, 10% Glycerin, 1% Triton X-100, 10 mM $Na_4O_7P_2$, protease inhibitor cocktail (cOmplete, EDTA free, Roche Diagnostics ref. 1187358001)]. Samples were sonicated 3 × 5 s (30% amplitude, Digital Sonifier W-250D, Branson Ultrasonics) and centrifuged at 13,000 rpm for 5 min at 4°C. The supernatant was stored at −80°C until use. Protein concentration was determined by Pierce BCA Protein Assay Kit (Thermo Fisher Scientific). Samples were separated by 4–12% NuPAGE Bis-Tris gels using NuPAGE 4xLDS sample buffer, NuPAGE 10x sample reducing agent and NuPAGE MES SDS running buffer (Invitrogen). Proteins were transferred onto PVDF membranes (0.2 µm, Biorad) and visualized using Clarity Western ECL Substrate (Biorad) and ChemiDoc MP Imaging System (Biorad).

Antibodies against APP and CTFs (rabbit polyclonal antibody against the APP C-terminus [6687], 1:1000 [32]), anti-Aβ (mouse, 1:3000, Covance, 6E10), anti BACE1 (rabbit, 1:1000, Cell Signalling, D10E5), anti-insulin-degrading enzyme [IDE] (rabbit, 1:5000, abcam, ab109538), anti-neprilysin (rabbit, 1:2500, Abcam, ab79423), anti-β-actin-HRP (mouse, 1:5000, abcam, ab20272), anti-mouse IgG HRP-linked Antibody (1:3000, Cell Signalling, 7076S) and anti-rabbit IgG HRP-linked Antibody (1:3000, Abcam, ab16824) were used.

## 2.8 | ELISA

For the quantification of $Aβ_{40}$ and $Aβ_{42}$ species in the soluble and insoluble olfactory bulb extracts, tissue of the olfactory bulb was homogenized (10% w/v) in 1XPBS + protease inhibitor cocktail (cOmplete, EDTA free, Roche Diagnostics) and sequentially extracted in 1XPBS (soluble fraction), 1XPBS + 0.1% Triton X-100 (membrane-bound fraction) and finally in 8 M guanidine hydrochloride solution. Protein concentration in

each fraction was measured with the Bradford reagent (Roti®-Quant, Roth) and enzyme-linked immunosorbent assay (ELISA) was performed using Human Aβ40 ELISA kit (Life Technologies, catalogue no. KHB3481) and Human Aβ42 ELISA kit (Life Technologies, catalogue no. KHB3441), according to the manufacturer's protocol.

## 2.9 | *In vivo* amyloid-β phagocytosis assay

Mice were injected intraperitoneally with methoxy-X04 (Tocris cat. no.4920) at 10 mg/kg bodyweight as described before [33]. Olfactory bulbs were isolated 3 h after methoxy-X04 injection and homogenized into single-cell suspension with a glass potter. The solution was filtered through a cell strainer (70 μm) and separated by 37% Percoll gradient centrifugation at 800 g for 30 min at 4°C. The cell suspension was collected and washed with 1XPBS. Fc receptor blocking antibody CD16/CD32 (1:200, clone 2.4G2, BD Bioscience) was applied to prevent unspecific binding, and dead cells were stained using the Fixable Viability Dye eFluor® 780 (1:1000, eBioscience) at 4°C for 20 min. Cells were washed in FACS buffer containing 1XPBS, 2% heat-inactivated FSC, 10 mM EDTA and then incubated with primary antibodies directed against CD11b (1:200, clone M1/70, Biolegend, cat. no. 101212), CD45 (1:200, clone 30-F11, Biolegend, cat. no. 103106), and a Dump gate was set to avoid contamination of peripheral myeloid and lymphoid cells by adding primary antibodies against anti-CD3 (1:300, clone 17A2, Biolegend, cat. no. 100220), anti-CD19 (1:300, clone 6D5, Biolegend, cat. no. 115520), anti-CD45R (1:300, clone RA3-6B2, BD Bioscience; cat. no. 552772), Ly6C (1:300, clone AL-21, BD Bioscience, cat. no. 560593) and Ly6G (1:300, clone 1A8, BD Bioscience, cat. no. 560601) for 20 min at 4°C. Percentage and mean fluorescent intensity of Dump methoxy-XO4$^+$ CD11b$^+$CD45$^{low}$ microglia were determined by flow cytometry using an FACS Canto II (BD Bioscience) and analysed with FlowJo software (Tree Star). WT mice injected with methoxy-X04 were used as negative controls to set the threshold of methoxy$^-$ cells. Corresponding isotype controls were used.

## 2.10 | Preparation of brain homogenates for intracerebral injections

Mouse brain homogenates were derived from 12-month-old plaque bearing heterozygous *APPPS1* transgenic mice and prepared as previously described [33–35]. Homogenate was obtained from the whole mouse brain. The brain tissue sample was freshly frozen and stored at −80°C until use. The sample was homogenized in sterile 1XPBS at 10% (w/v) and sonicated 3 × 5 s (30% amplitude, Digital Sonifier W-250D, Branson Ultrasonics). The crude brain homogenate was centrifuged for 5 min (at 3000 × *g*, 4°C) and the supernatant was stored at −80°C until use.

## 2.11 | Intracerebral stereotactic injections

Mice were anaesthetized via intraperitoneal injection of a mixture of ketamine (100 mg/kg body weight) and xylazine (5 mg/kg body weight) in saline. For bilateral stereotactic injections of brain homogenates, a Hamilton syringe was placed into the olfactory bulb (AP + 5.0 mm; L ± 1.0 mm; DV − 1.0 mm) of 8-week-old male *APPPS1* and *APPPS1 × [A30P]aSYN* mice. Mice were injected with *APPPS1* transgenic brain homogenate (3 μl per hemisphere at an injection speed of 1 μl/min). After each injection, the needle was kept in place for an additional 2 min before it was slowly withdrawn. The surgical site was cleaned with sterile saline and the incision sutured. Mice were monitored until recovery from anaesthesia and incubated for 12 weeks.

## 2.12 | Preparation of cortical cell suspensions for intracerebral grafting

Primary cortical neurons were isolated from C57BL/6 WT mice at embryonic days 16–17. Cortical samples were isolated and processed to single-cell solution on ice, trypsinized for 10 min with 0.05% Trypsin-EDTA (Gibco) at 37°C and washed three times in HBSS (Gibco). Cells were then triturated in DMEM (Gibco) by pipetting up and down until the suspension was homogenous and maintained on ice until further use for intracerebral injection [22].

## 2.13 | Intracerebral grafting

Mice were anaesthetized via intraperitoneal (i.p.) injection with a mixture of ketamine (100 mg/kg body weight) and xylazine (5 mg/kg body weight) dissolved in saline. For bilateral stereotactic transplantation of neuronal cell suspension, a Hamilton syringe was placed into the cortex (AP + 1.8 mm, L ± 1.5 mm, DV − 1.3 mm) of 8-week-old transgenic *APPPS1* and *APPPS1 × [A30P] aSYN* animals. Mice were injected with a volume of 3 μl (approximately 20,000 cells) per hemisphere at an injection speed of 1 μl/min. After each injection, the needle was kept in place for an additional 1 min before it was slowly withdrawn. The surgical site was cleaned with sterile saline and the incision sutured. Mice were monitored until recovery from anaesthesia and incubated for 4 and 8 weeks. For intra-cerebral grafting experiments, only female mice were used.

## 2.14 | Statistical analysis

GraphPad Prism 7 (GraphPad Software, Inc.) was used for statistical analysis. All data sets were tested for normality with the D'Agostino-Pearson omnibus K2 normality test with a significance level set to $p = 0.05$ before the appropriate parametric or non-parametric statistical comparison test was carried out. Student's $t$ test or Mann–Whitney test was applied. Reported values are means ± SEM. Significance level $\alpha$ was set to 0.05. $*p < 0.05$, $**p < 0.01$, and $***p < 0.001$.

## 3 | RESULTS

### 3.1 | Similar plaque load in 4-month-old *APPPS1* and *APPPS1 × [A30P]aSYN* mice

Based on our previous finding that hippocampal plaque load was reduced because of the presence of α-syn in *APPPS1 × [A30P]aSYN* mice [22], we first investigated the endogenous Aβ plaque load in the olfactory bulb of 4-month-old *APPPS1*, *APPPS1 × [A30P]aSYN* and WT mice (Figure 1A). As expected, no Aβ plaques were evident in WT mice (Figure 1A). By using the anti-Aβ-specific antibody 6E10 to visualize Aβ, and Thiazine red that solely stains dense-core Aβ plaques, we could not observe any differences in Aβ load between *APPPS*1 and *APPPS1 × [A30P]aSYN* mice (Figure 1A–C). In accordance with these data, we detected comparable soluble and insoluble Aβ$_{40}$ and Aβ$_{42}$ levels in both mouse models using ELISA measurements (Figure 1D,E). Further biochemical analyses by Western blot revealed no differences in APP or CTF-fragment (CTF-α and CTF-β) levels as well as levels of BACE1 secretase (Figure 1F,G), suggesting that APP processing was not affected in those mice at 4 months of age. Finally, the analyses of IDE and Neprilysin enzymes, which are both involved in the degradation of Aβ, uncovered again similar levels in *APPPS1* and *APPPS1 × [A30P]aSYN* mice (Figure 1G).

### 3.2 | α-syn diminishes Aβ plaque load in 8-month-old *APPPS1 × [A30P]aSYN* mice

In order to assess the potential effect of α-syn on Aβ plaque formation, we analysed Aβ plaque pathology in the olfactory bulb at a more advanced stage of the Aβ polymerization process, represented by 8-month-old *APPPS1* and A*PPPS1 × [A30P]aSYN* mice (Figure 2A). Indeed, olfactory bulb total and compact Aβ plaque burden in *APPPS1 × [A30P]aSYN* mice was reduced compared with that of *APPPS1* transgenic animals based on immunofluorescent stainings (Figure 2B,C). In accordance with these results, we found significantly reduced soluble and insoluble Aβ$_{40}$ and Aβ$_{42}$ species in those mice (Figure 2D,E). In order to examine whether

the reduced Aβ plaque load in *APPPS1 × [A30P]aSYN* mice is a consequence of decreased APP processing or increased Aβ degradation, we performed Western blot analyses. Likewise, we detected less Aβ in the presence of α-syn in *APPPS1 × [A30P]aSYN* mice by probing the membrane with a 6E10 antibody (Figure 2F). Moreover, the levels of the CTF fragments (CTF-α and CTF-β) were affected in a related manner, while full-length APP levels were similar in both groups, suggesting inhibition of Aβ peptide formation by α-syn. Additionally, BACE1 levels were slightly reduced in *APPPS1 × [A30P]aSYN* mice compared to *APPPS1* mice (Figure 2G), implying a potential suppression of BACE1 expression in these mice. Concurrently, we detected higher IDE levels in double-transgenic mice, while Neprilysin was unchanged (Figure 2G), referring to an increased Aβ degradation in *APPPS1 × [A30P]aSYN* compared to *APPPS1* mice which in turn correlated with decreased Aβ levels in these double-transgenic mice.

Next, we sought to study whether this effect endured over a prolonged period and analysed the Aβ plaque load in 12-month-old *APPPS1* and *APPPS1 × [A30P]aSYN* mice (Figure S1A). However, at this advanced age, no significant differences between neither the total or compact Aβ plaque burden were evident (Figure S1B,C) and we also found similar levels of soluble and insoluble Aβ$_{40}$ and Aβ$_{42}$ species in these mice (Figure S1D,E). Furthermore, immunoblots probed with Aβ-specific antibodies revealed again no differences in Aβ levels as well as APP processing between 12-month-old *APPPS1* and *APPPS1 × [A30P]aSYN* mice (Figure S1F). Together, these findings demonstrate that the α-syn-mediated inhibitory effect becomes especially evident in 8-month-old mice but disappears with the higher age of the mice.

### 3.3 | Presence of α-syn does not alter the phagocytic capacity of microglia

To investigate whether diminished Aβ pathology is a consequence of enhanced microglial phagocytosis because of α-syn overexpression in 8-month-old *APPPS1 × [A30P]aSYN* mice, we analysed *in vivo* Aβ uptake by microglial cells using methoxy-X04 staining and flow cytometry as previously described [33] (Figure 3A). FACS dot plots and respective histograms from *APPPS1* and *APPPS1 × [A30P]aSYN* mice revealed no significant difference in Aβ phagocytosis (Figure 3B,C). Nevertheless, we noticed a slightly higher percentage of microglia containing methoxy-X04 in *APPPS1 × [A30P]aSYN* mice, but this trend did not reach significance (Figure 3D). Next, we quantified the number of Aβ plaque-associated Iba1^{+} microglia cells and found again no difference in the number of plaque-associated microglia cells in both groups (Figure 3E,F). Furthermore, quantitative assessment of CD68 immunoreactivity in *APPPS1* and *APPPS1 × [A30P]aSYN* mice (Figure 3G)
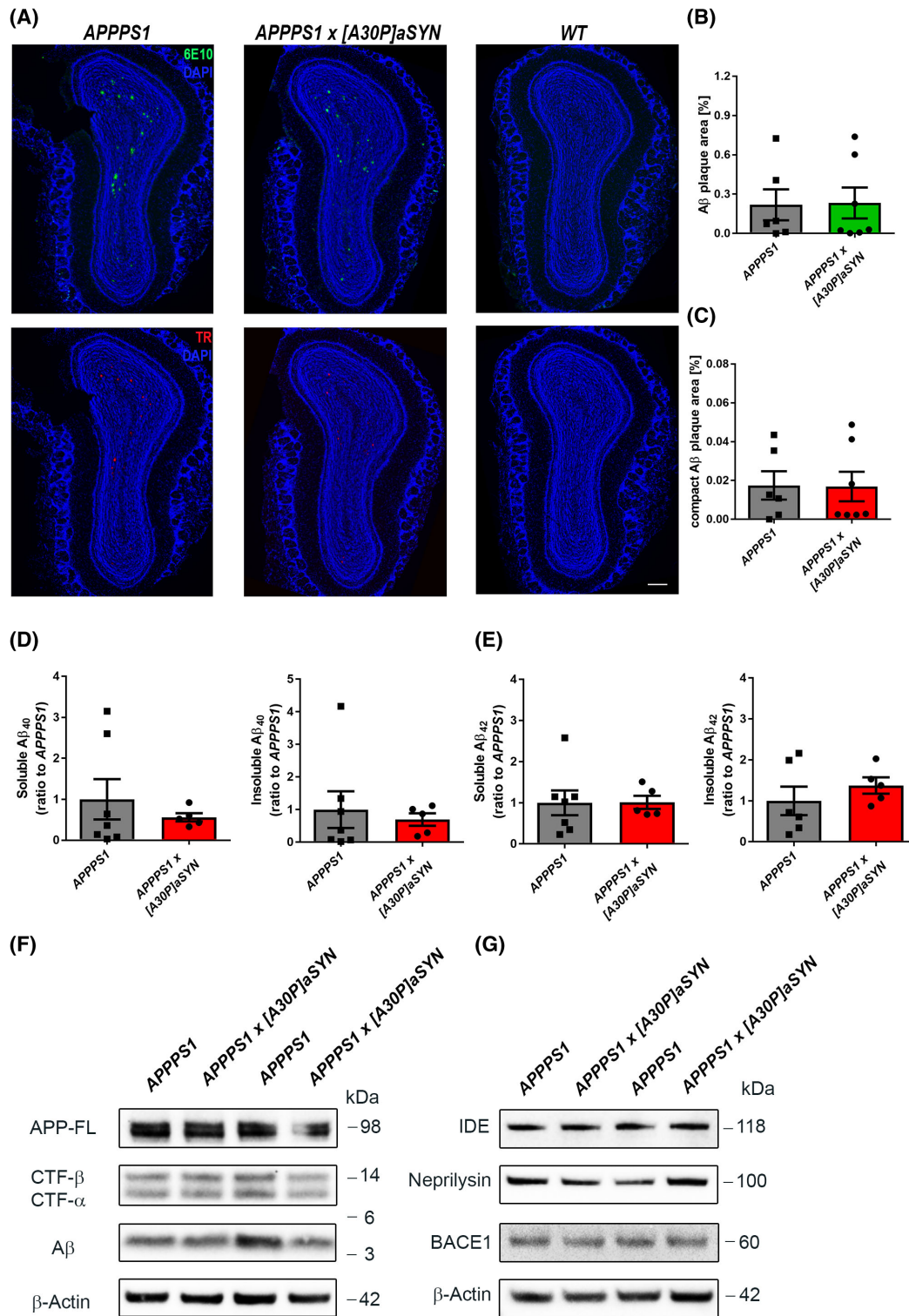
**FIGURE 1** Similar Aβ plaque burden in the olfactory bulb of 4-month-old *APPPS1* and *APPPS1* × *[A30P]aSYN* mice. (A) Representative images of immunofluorescent staining of Aβ plaques (6E10, green and DAPI, blue) and compact Aβ plaque load [Thiazine red (TR), red and DAPI, blue] in olfactory bulbs of 4-month-old male *APPPS1*, *APPPS1* × *[A30P]aSYN* and *WT* mice. Scale bar represents 200 μm. (B) Quantification of Aβ plaque load (as Aβ-positive area fraction based on 6E10 staining). (C) Quantification of compact Aβ plaque burden based on TR staining. Each symbol represents data from one mouse (*APPPS1*: n = 6, *APPPS1* × *[A30P]aSYN*: n = 7). Data are presented as mean ± SEM. (D) Assessment of soluble and insoluble Aβ40 and (E) soluble and insoluble Aβ42 peptide fractions of olfactory bulb brain extracts from 4-month-old *APPPS1* and *APPPS1* × *[A30P]aSYN* mice by Enzyme-linked immunosorbent assays (ELISA). Each symbol represents data from one mouse (*APPPS1*: n = 6–7, *APPPS1* × *[A30P]aSYN*: n = 5). Data are presented as mean ± SEM. Data were normalized to *APPPS1*. (F) Representative immunoblots of olfactory bulb brain extracts from 4-month-old male *APPPS1* and *APPPS1* × *[A30P]aSYN* mice. Immunoblots were probed with antibodies that recognize full-length APP, CTFβ and CTFα (6687), Aβ (6E10). (G) insulin-degrading enzyme (IDE), Neprilysin and β-secretase 1 (BACE1). β-Actin was used as a loading control

confirmed the aforementioned results and revealed no difference between the two groups (Figure 3H).

Taken together, these findings argue against the possibility that decreased Aβ plaque load in 8-month-old *APPPS1 × [A30P]aSYN* compared to *APPPS1* mice might be attributable to an increased phagocytic capacity of microglial cells.

## 3.4 | α-syn significantly reduces Aβ seeding and inhibits the formation of Aβ pathology in *APPPS1 × [A30P]aSYN* grafts

We previously demonstrated that α-syn acts as an inhibitor for Aβ plaque formation *in vivo* in the hippocampus of *APPPS1* mice co-expressing α-syn [22]. By applying the well-established Aβ seeding model to the olfactory bulb (Ziegler-Waldkirch et al., unpublished data) [36], we examined the effect of additional α-syn on seed-induced Aβ plaque formation in the olfactory bulb of *APPPS1 × [A30P]aSYN* mice and analysed the Aβ seeding pattern after 12 weeks of incubation (Figure 4A). In accordance with our previous results, Aβ seeding was mainly evident in the granular cell layer of the olfactory bulb (Figure 4B). Quantitative analysis of seed-induced Aβ deposits revealed a significant seeding area reduction of approximately 50% in *APPPS1 × [A30P]aSYN* (Figure 4C), supporting the attenuating effect of α-syn during Aβ formation *in vivo* [22].

In order to test the hypothesis with a different approach, we took advantage of embryonic WT neurons transplanted into either *APPPS1* or *APPPS1 × [A30P]aSYN* mice [22, 37] and examined the grafts for the presence of Aβ deposits after 4 and 8 weeks of incubation (Figure 4D,E). We already demonstrated earlier that grafts derived from *aSYN* mice incorporated no or less Aβ material than grafts originated from WT mice [22]. In this case, the presence of α-syn in the surrounding host tissue of *APPPS1 × [A30P]aSYN* mice seemed to have only an effect on the formation of Aβ plaques within the grafts 8 weeks after injection while after 4 weeks the plaques that formed within the grafts were alike (Figure 4F). However, after 8 weeks of WT neuron injections, a significant decrease of Aβ plaque numbers was evident in *APPPS1 × [A30P]aSYN* mice (Figure 4G).

Together, both findings confirm the suppressive role of α-syn for Aβ plaque formation in mice co-expressing both pathologies.

## 3.5 | Presence of α-syn ameliorates olfactory deficits in *APPPS1 × [A30P]aSYN* mice

Next we moved on to assess olfactory behaviour and a possible correlation between the endogenous Aβ plaque load and olfactory function in *APPPS1* and *APPPS1 × [A30P]aSYN* mice at the age of 4 and 8 months. For this purpose, we performed the buried food and the olfactory avoidance test with *APPPS1*, *APPPS1 × [A30P]aSYN* and WT mice (Figure 5A–C). In accordance with similar Aβ plaque burden in the olfactory bulb of 4-month-old mice (Figure 1B,C), we did not detect any differences in olfactory performance of *APPPS1* and *APPPS1 × [A30P]aSYN* mice (Figure 5B,C) that were comparable to those of WT mice at the same age. However, 8-month-old *APPPS1* mice needed significantly more time to find the buried food (Figure 5B) and spent significantly more time in the avoidance area compared to *APPPS1 × [A30P]aSYN* and WT mice (Figure 5C), implying olfactory deficits in *APPPS1* mice at this age. Furthermore, compared to *WT* littermates, *APPPS1 × [A30P]aSYN* mice behaved significantly different in the buried food test but not in the olfactory avoidance test (Figure 5B,C). These results indicate that lowered Aβ burden in the olfactory bulb caused by the presence of α-syn, indeed, led to an improved olfactory performance.

We hypothesized that olfactory deficits in 8-month-old mice may differ depending on the severity of plaque-associated pathology. Therefore, the number of projection neurons in form of mitral cells was evaluated first. However, no significant difference between *APPPS1* and *APPPS1 × [A30P]aSYN* mice could be detected neither with the commonly used Reelin-specific antibody (Figures S2A,B) nor with NeuroTrace staining (green fluorescent Nissl stain) (Figure S2C,D).

Finally, we investigated plaque-associated toxicity that is represented by surrounding dystrophic neurites that are normally embedded within dense-core plaques or in their very close vicinity. Quantitative assessment of Lamp2 immunoreactivity [38] revealed indeed a significant decrease of dystrophic structures in *APPPS1 × [A30P]aSYN* mice compared to *APPPS1* transgenic mice (Figure 5D,E), suggesting that the concomitance of Aβ and α-syn might extenuate local neural system destruction of the olfactory pathway in the granular cell layer.

## 4 | DISCUSSION

Overlap between α-syn and Aβ pathologies was frequently described as an important phenomenon occurring in several neurodegenerative diseases [3, 8–12,], generating the problem of recognizing DLB as a distinct age-associated neurodegenerative dementia. Several *in vitro* and *ex vivo* studies suggested a direct interaction between both peptides [13–17] and an inhibitory effect of α-syn on Aβ plaque formation in the hippocampus of *APPPS1 × [A30P]aSYN* mice [22], while the consequences of simultaneous α-syn and Aβ pathologies on the olfactory system are still unknown.

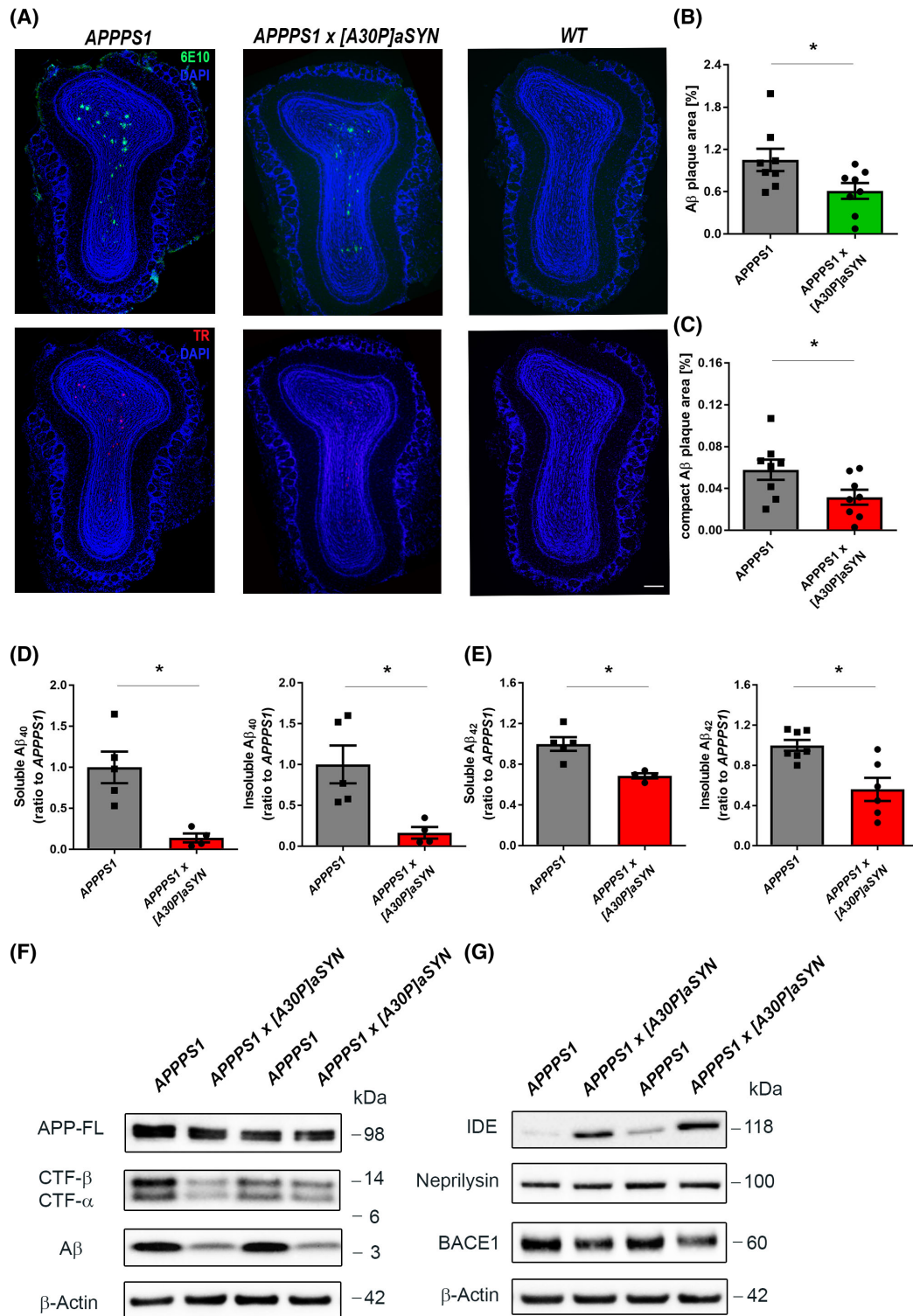Here we first examined the effect of α-syn on Aβ burden and Aβ levels in the olfactory bulb of 4-, 8- and

**FIGURE 2** Decreased Aβ plaque load in the olfactory bulb of 8-month-old *APPPS1 × [A30P]aSYN* mice. (A) Immunofluorescent staining of Aβ plaques (6E10, green and DAPI, blue) and compact Aβ plaque load [Thiazine red (TR), red and DAPI, blue] in olfactory bulbs of 8-month-old male *APPPS1*, *APPPS1 × [A30P]aSYN* and *WT* animals. Scale bar represents 200 μm. (B) Quantification of 6E10 immunostaining as Aβ-positive area fraction. Each symbol represents data from one mouse. Data are presented as mean ± SEM. Significant differences were determined by the Mann–Whitney test ($p = 0.0499$). (C) Quantification of TR staining. Each symbol represents data from one mouse. Data are presented as mean ± SEM. Significant differences were determined by the unpaired $t$ test ($p = 0.0464$). (*APPPS1*: $n = 8$, *APPPS1 × [A30P]aSYN*: $n = 8$) (D) Enzyme-linked immunosorbent assay (ELISA) for soluble and insoluble $A\beta_{40}$ and (E) soluble and insoluble $A\beta_{42}$ peptide fractions of olfactory bulb brain extracts from 8-month-old *APPPS1* and *APPPS1 × [A30P]aSYN* mice. Each symbol represents data from one mouse (*APPPS1*: $n = 5$–7, *APPPS1 × [A30P]aSYN*: $n = 4$–6). Data were normalized to *APPPS1*. Data are presented as mean ± SEM. Significant differences were determined by the Mann–Whitney test [$p = 0.0159$; $p = 0.0221$ (insoluble $A\beta_{42}$)]. (F) Representative immunoblots of olfactory bulb brain extracts from 8-month-old male *APPPS1* and *APPPS1 × [A30P]aSYN* mice. Immunoblots were probed with antibodies that recognize full-length APP, CTFβ and CTFα (6687), Aβ (6E10), (G) insulin-degrading enzyme (IDE), Neprilysin and β-secretase 1 (BACE1). β-Actin was used as a loading control
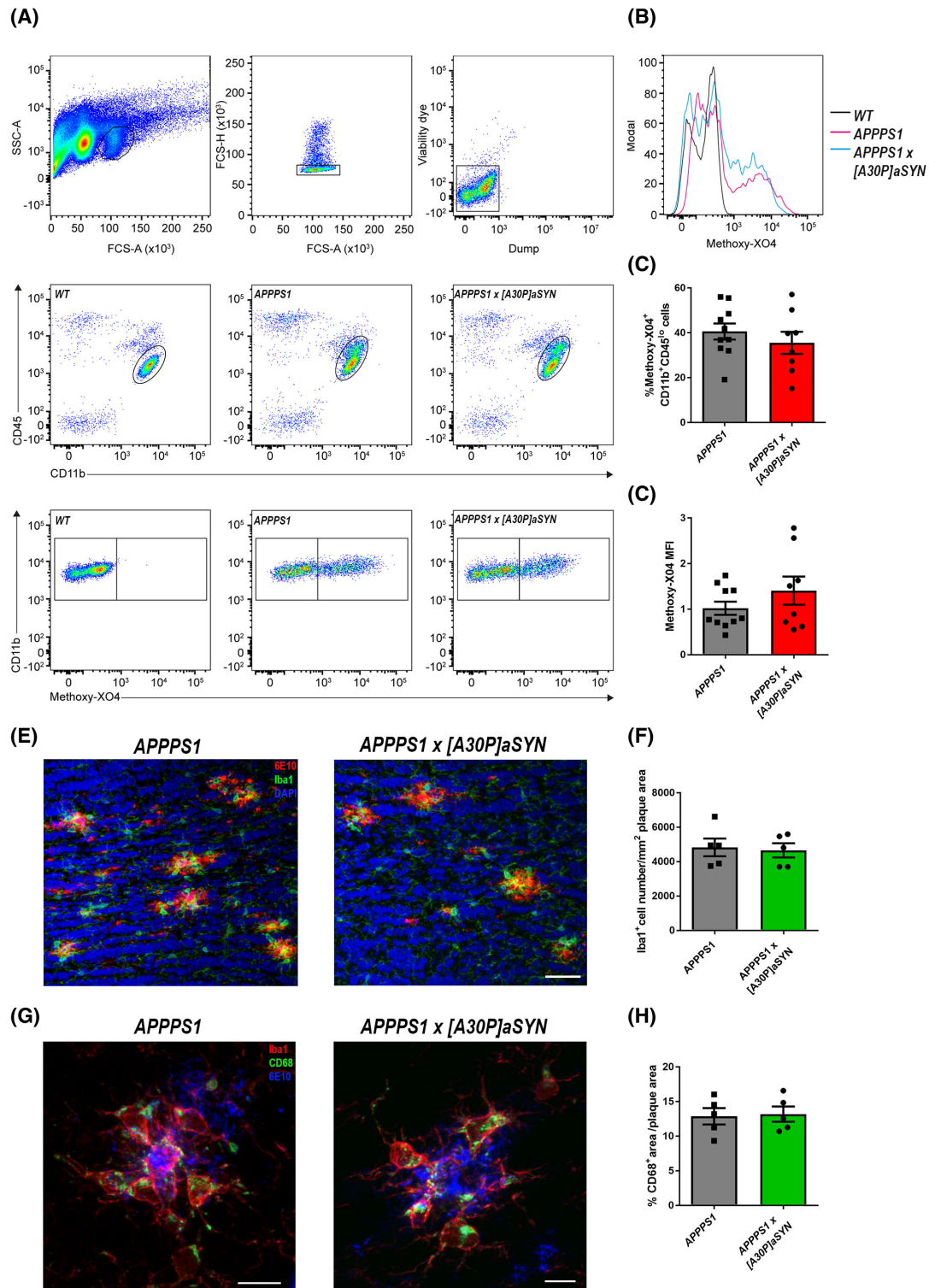
12-month-old *APPPS1* and *APPPS1* × *[A30P]aSYN* mice. As a result of high variation in 4-month-old mice, no significant differences were observed implicating that this age represents an early event in the elongation phase of the nucleation-dependent Aβ polymerization cascade [39]. However, α-syn significantly diminished Aβ plaque burden and lowered the amount of soluble and insoluble $A\beta_{40}$ and $A\beta_{42}$ species in the olfactory bulb of 8-month-old *APPPS1* × *[A30P]aSYN* mice, confirming a similar observation that has been made in the hippocampus of those same mice [22]. Further analysis of 12-month-old *APPPS1* and *APPPS1* × *[A30P]aSYN* mice revealed again no difference despite their very large Aβ burden, suggesting that the suppressive effect of α-syn on Aβ plaque formation is abolished at an advanced age.

**FIGURE 3**    Presence of α-synuclein does not influence the number and phagocytic capacity of microglial cells in 8-month-old *APPPS1 × [A30P]aSYN* mice. (A) Gating of Dump⁻CD11b⁺CD45$^{low}$ methoxy-X04⁺ microglia and representative FACS dot plots from 8-month-old male *APPPS1* and *APPPS1 × [A30P]aSYN* mice and age-matched *WT* controls. (B) Representative cytometric graph of Dump⁻CD11b⁺CD45$^{low}$ methoxy-X04⁺ microglial cells from *WT* (black line), *APPPS1* (red line) and *APPPS1 × [A30P]aSYN* (blue line). (C) Quantification of percentages (%) of Dump⁻CD11b⁺CD45$^{low}$ methoxy-X04⁺ microglial cells from olfactory bulb of 8-month-old *APPPS1* (*n* = 10) and *APPPS1 x [A30P]aSYN* (*n* = 8) mice. Each symbol represents data from one mouse. Data are presented as mean ± SEM. Data are pooled from two independent experiments. (D) Quantification of the methoxy-X04 mean fluorescence intensity (MFI). Data were normalized to *APPPS1*. Each symbol represents data from one mouse (*APPPS1*: *n* = 10, *APPPS1 × [A30P]aSYN*: *n* = 8). Data are presented as mean ± SEM. Data are pooled from two independent experiments. (E) Representative confocal images of Iba1⁺ (green) microglia cells surrounding Aβ plaques (6E10, red) on olfactory bulb sections of *APPPS1* and *APPPS1 × [A30P]aSYN* mice. Nuclei are counterstained by DAPI (blue). Scale bar represents 50 μm. (F) Quantification of plaque-associated Iba1⁺ microglial cells. Each symbol represents data from one mouse (*APPPS1*: *n* = 5, *APPPS1 × [A30P]aSYN*: *n* = 5). Data are presented as mean ± SEM. (G) Representative confocal images of CD68 (6E10 blue, Iba1 red and CD68 green). Scale bars represent 10 μm. (H) Quantitative assessment of CD68 immunoreactivity in *APPPS1* (*n* = 5) and *APPPS1 × [A30P]aSYN* (*n* = 5) mice. Each symbol represents data from one mouse. Data are presented as mean ± SEM

In line with recent *in vitro* work that demonstrated that α-syn interacts with IDE and is able to increase its proteolytic activity [40, 41], we indeed found an upregulation of IDE in double-transgenic mice that consequently led to lower Aβ levels. Future studies will need to address the exact cause for this increase in IDE. As we found a strong decrease of CTF's (CTF-α and CTF-β) and even a slight reduction of BACE1 levels in mice presenting α-syn pathology, these experiments imply that the observed reduced amyloid plaque density was caused by alterations in APP processing and production because of the presence of α-syn.

Several studies demonstrated that microglial cells crucially contribute to the clearance and phagocytosis of amyloid-β [33, 42–45,]. Likewise, α-syn has been demonstrated to activate microglial cells *in vitro* [46–48], which prompted us to hypothesize that Aβ plaque burden was alleviated in *APPPS1 × [A30P]aSYN* mice through effective phagocytosis performed by activated microglia. However, no evidence for higher phagocytic activity of microglial cells isolated from double-transgenic mice was found in methoxy-X04-FACS analyses. Additionally, the number of plaque-associated microglial cells and CD68 immunoreactivity did not differ among both mouse models. Given that the IDE enzyme is also secreted by microglial cells [49], this could provide a reasonable explanation for higher IDE levels in *APPPS1 × [A30P] aSYN* mice.

We had previously shown that α-syn diminished Aβ seeding capacity in the hippocampus of *APPPS1 × [A30P] aSYN* mice, indicating an inhibitory role for α-syn [22]. Moreover, we established the olfactory bulb as a new brain region to study seed-induced Aβ plaque formation *in vivo* (Ziegler-Waldkirch et al., unpublished data). By combining both approaches via inoculation of Aβ-rich brain extracts in the olfactory bulb of pre-depositing mice, we could show that the Aβ seeding area was significantly decreased in the olfactory bulb of *APPPS1 x [A30P]aSYN* compared to *APPPS1* mice. Along the same lines, grafting experiments supported the inhibitory role of α-syn as the number of plaques per graft was significantly reduced in WT grafts of *APPPS1 × [A30P] aSYN* mice 8 weeks post-transplantation compared to

*APPPS1* mice. Most likely, the effect of α-syn becomes evident when a certain threshold of Aβ plaque load is present in the host animal that might not yet be reached 4 weeks post-transplantation. Thus, the present results corroborate our previous finding [22] that the presence of α-syn slows down Aβ plaque formation and interferes with the aggregation process of Aβ.

Multiple lines of evidence indicate a negative correlation between increasing Aβ plaque load and decreasing ability to smell [23, 24]. Furthermore, our previous work revealed a link between seed-induced Aβ deposition, representing early stages of plaque formation, and subsequent olfactory deficits in 5xFAD mice (Ziegler-Waldkirch et al., unpublished data). We hence set out to investigate potential olfactory deficits and whether the extent of Aβ pathology present in *APPPS1* and *APPPS1 × [A30P]aSYN* mice might impact olfactory performance differently. Strikingly, 8-month-old animals, carrying additional overexpression of α-syn, developed olfactory deficits that were less pronounced than the ones in *APPPS1* mice. This different ability to smell was not evident in 4-month-old mice with lower Aβ plaque load in both genotypes, which might explain why no distinction in olfactory performance was identified. In accordance with the above-mentioned literature, we therefore confirmed the negative correlation between olfaction deficits and increasing deposition of Aβ pathology.

Examinations on the influence of Aβ on bulbar neuronal network and functionality are of great interest [24, 50, 51]. Evaluation of mitral cell numbers yielded only a slight trend but did not reach significance to decreased mitral cell numbers in *APPPS1* mice, implying a negative impact of Aβ pathology on the bulbar network. On the contrary, analysis of Lamp2 immunoreactivity, that is associated with dystrophic neurites [38], revealed a significant decrease in double-transgenic animals, suggesting the destruction of network in the granular cell layer potentially leading to olfactory deficits seen in *APPPS1* mice. More work on the bulbar network is necessary, in particular, the question of how Aβ exactly influences the bulbar network on a cellular and functional level needs to be addressed in more detail.
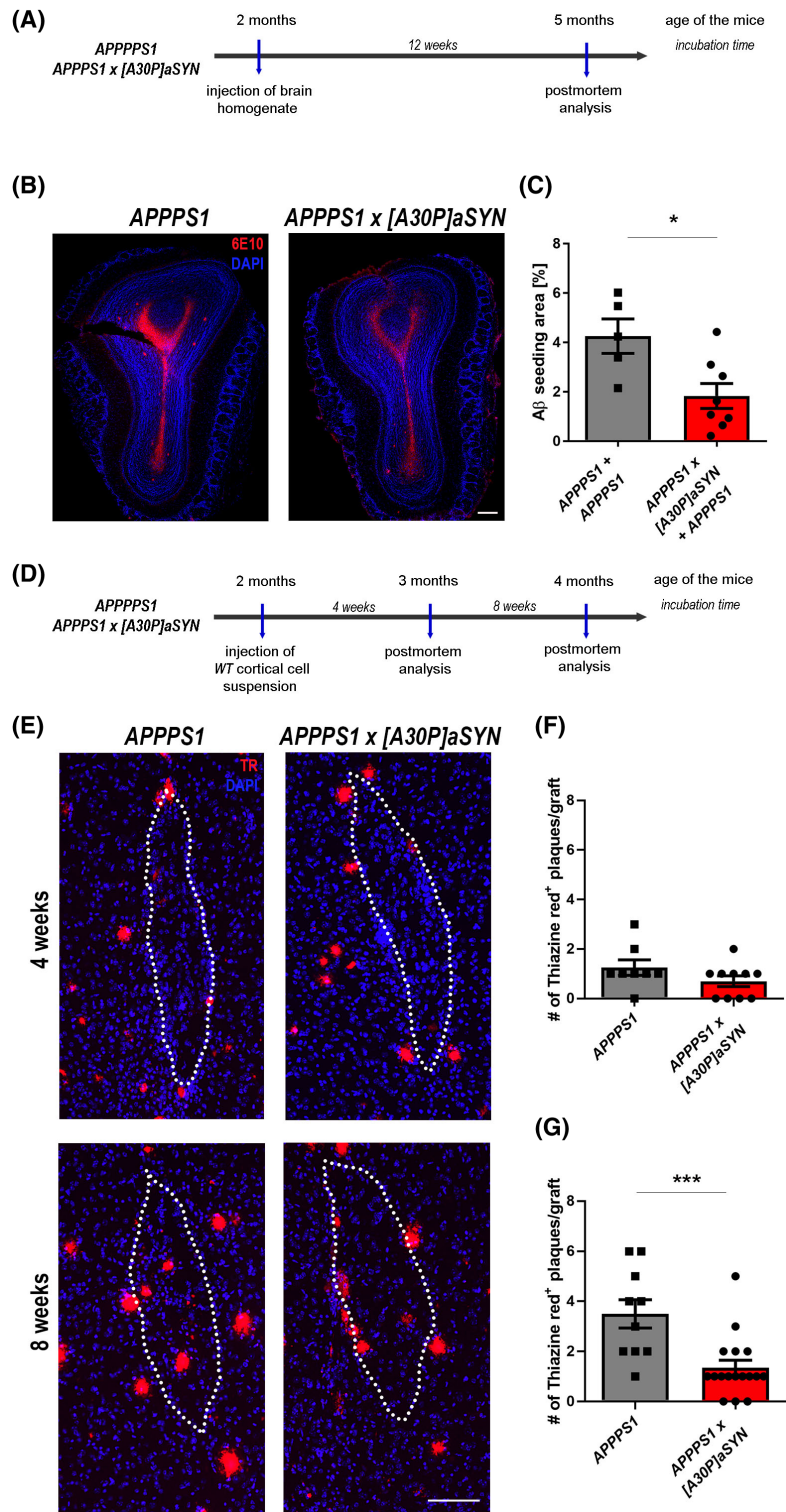
**FIGURE 4** α-synuclein interferes with the formation of Aβ deposits. (A) Scheme of Aβ seeding experiments with *APPPS1* and *APPPS1 × [A30P]aSYN* mice. (B) Representative images of immunofluorescent staining of Aβ plaques (6E10, red) in the olfactory bulb of male *APPPS1* and *APPPS1 × [A30P]aSYN* mice inoculated with brain extracts from aged *APPPS1* mice and sacrificed at the age of 20 weeks (12 weeks post-injection). Scale bar represents 200 μm. (C) Quantification of Aβ load as % of total olfactory bulb area. Each symbol represents data from one mouse (*APPPS1*: $n = 5$, *APPPS1 × [A30P]aSYN*: $n = 8$). Data are presented as mean ± SEM. Significant differences were determined by the Mann–Whitney test ($p = 0.0295$). (D) Scheme of intracerebral grafting experiments with *APPPS1* and *APPPS1 × [A30P]aSYN* mice. (E) Images of TR$^+$ (red) Aβ deposits in *WT* grafts transplanted in female *APPPS1* and *APPPS1 × [A30P]aSYN* host animals 4 and 8 weeks after inoculation. Nuclei are counterstained with DAPI (blue). Grafts are indicated by the dashed line (white). Scale bar represents 100 μm. (F) Quantification of the number of Aβ plaques per graft in *APPPS1* ($n = 8$) and *APPPS1 × [A30P]aSYN* ($n = 10$) hosts 4 weeks after transplantation of *WT* grafts. Each symbol represents data from one graft. Data are presented as mean ± SEM. (G) Quantification of TR$^+$ plaques within grafts after 8 weeks of neuronal cell injection. Each symbol represents data from one graft (*APPPS1*: $n = 10$, *APPPS1 × [A30P]aSYN*: $n = 17$). Data are presented as mean ± SEM. Significant differences were determined by the Mann–Whitney test ($p = 0.0008$)
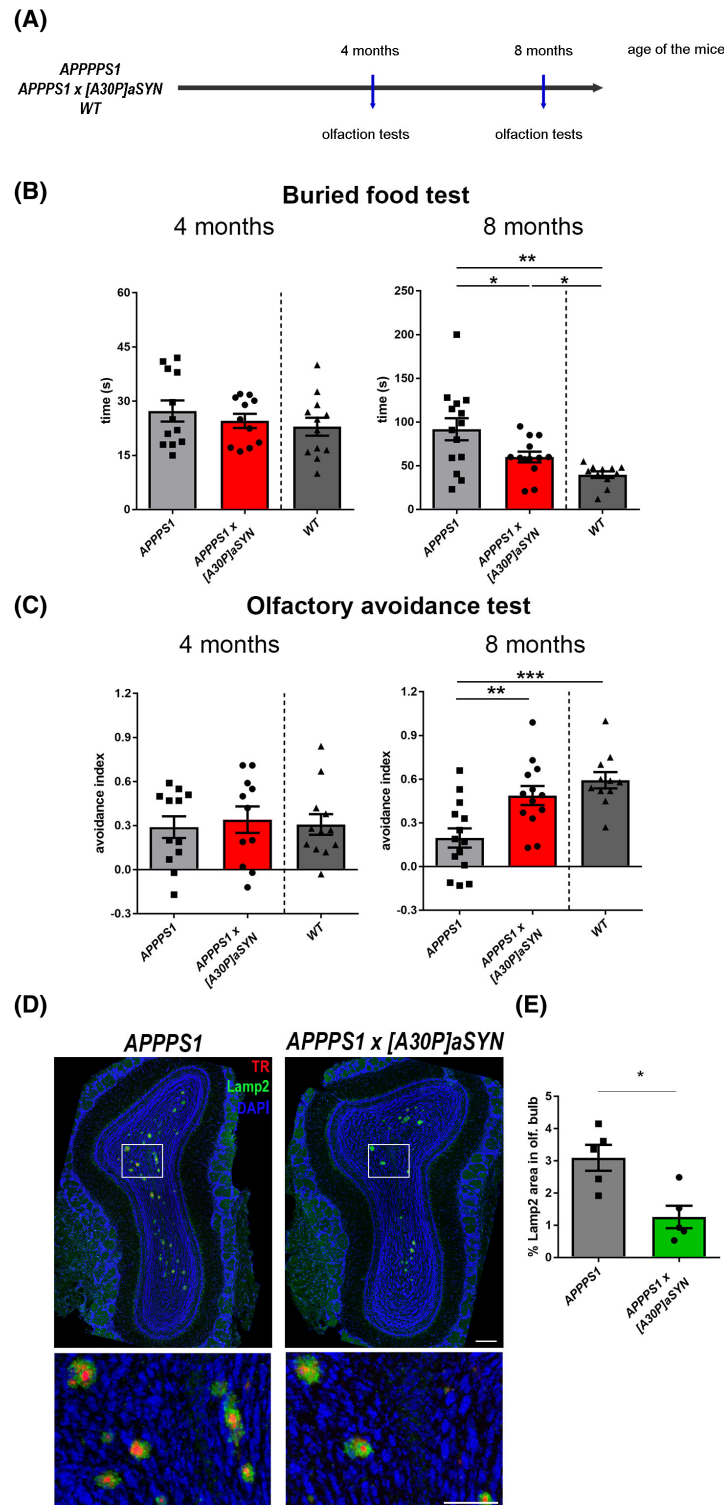
**FIGURE 5** Olfactory performance of *APPPS1 × [A30P]aSYN* animals. (A) Scheme of experimental protocol for olfaction tests with *APPPS1*, *APPPS1 × [A30P]aSYN* and *WT* mice. (B) Data obtained from buried food test from 4- and 8-month-old *APPPS1*, *APPPS1 × [A30P]aSYN* and *WT* mice. Each symbol represents data from one mouse (4 months: *APPPS1*: $n = 12$, *APPPS1 × [A30P]aSYN*: $n = 11$, *WT*: $n = 12$; 8 months: *APPPS1*: $n = 14$, *APPPS1 × [A30P]aSYN*: $n = 13$, *WT*: $n = 11$). Data are presented as mean ± SEM. Significant differences were determined by the unpaired *t* test ($p = 0.0362$, $p = 0.0130$, $p = 0.0017$). (C) Data obtained from olfactory avoidance test from 4- and 8-month-old *APPPS1*, *APPPS1 × [A30P]aSYN* and *WT* mice. Each symbol represents data from one mouse (4 months: *APPPS1*: $n = 12$, *APPPS1 × [A30P]aSYN*: $n = 11$, *WT*: $n = 12$; 8 months: *APPPS1*: $n = 14$, *APPPS1 × [A30P]aSYN* $n = 13$, *WT*: $n = 11$). Data are presented as mean ± SEM. Significant differences were determined by the unpaired *t* test ($p = 0.0043$, $p = 0.0002$). (D) Representative images of amyloid plaques (TR, red) surrounded by dystrophic neurites (Lamp2, green). Nuclei were counterstained with DAPI (blue). Scale bars represent 200 μm. (**E**) Quantification of immunofluorescent Lamp2 staining. Each symbol represents data from one mouse (*APPPS1*: $n = 5$, *APPPS1 × [A30P]aSYN*: $n = 5$). Data are presented as mean ± SEM. Significant differences were determined by the Mann–Whitney test ($p = 0.0317$)

# 5 | CONCLUSION

In conclusion, our study elucidates an inhibitory role of α-syn on Aβ plaque formation in the olfactory bulb of *APPPS1 × [A30P]aSYN* mice, further leading to the amelioration of olfactory deficits in mice harbouring both α-syn and Aβ pathologies. Together, our findings provide evidence for the possibility to differentiate between neurodegenerative diseases with concomitant α-syn and Aβ pathologies.

## CONFLICT OF INTEREST
The authors declare no competing interests.

## AUTHOR CONTRIBUTIONS
Marina Friesen, Stephanie Ziegler-Waldkirch and Melanie Meyer-Luehmann conceived and planned the experiments. Marina Friesen contributed to all aspects of the experiments and data analysis. Milena Egenolf, Paolo d'Errico, Christina Helm, Charlotte Mezö, Nikolaos Dokalis, Daniel Erny, Natalie Katzmarski, Romina Coelho and Desirée Loreth assisted with the experimental work. Marina Friesen, MP and Melanie Meyer-Luehmann discussed the results. Marina Friesen and Melanie Meyer-Luehmann wrote the manuscript and Melanie Meyer-Luehmann supervised the project. The authors read, edited and approved the manuscript.

## CONSENT FOR PUBLICATION
All authors consented to the publication of the manuscript.

## ETHICAL APPROVAL AND CONSENT TO PARTICIPATE
Not applicable.

## DATA AVAILABILITY STATEMENT
The data that support the findings of this study are available from the corresponding author upon reasonable request.

## ORCID
*Daniel Erny* https://orcid.org/0000-0001-6000-8838
*Desirée Loreth* https://orcid.org/0000-0003-0827-149X
*Melanie Meyer-Luehmann* https://orcid.org/0000-0003-3661-2220

## REFERENCES
1. Forno LS. Neuropathology of Parkinson's disease. J Neuropathol Exp Neurol. 1996;55:259–72. https://doi.org/10.1097/00005072-199603000-00001

2. Holtzman DM, Morris JC, Goate AM. Alzheimer's disease: the challenge of the second century. Sci Transl Med. 2011;3:77sr1. https://doi.org/10.1126/scitranslmed.3002369

3. McKeith I, Mintzer J, Aarsland D, Burn D, Chiu H, Cohen-Mansfield J, et al.; International Psychogeriatric Association Expert Meeting on DLB. Dementia with Lewy bodies. Lancet Neurol. 2004;3:19–28.

4. Pollanen MS, Dickson DW, Bergeron C. Pathology and biology of the Lewy body. J Neuropathol Exp Neurol. 1993;52:183–91. https://doi.org/10.1097/00005072-199305000-00001

5. Spillantini MG, Schmidt ML, Lee VM-Y, Trojanowski JQ, Jakes R, Goedert M. α-Synuclein in Lewy bodies. Nature. 1997;388:839–40. https://doi.org/10.1038/42166

6. Lippa CF, Duda JE, Grossman M, Hurtig HI, Aarsland D, Boeve BF, et al.; DLB/PDD Working Group. DLB and PDD boundary issues: diagnosis, treatment, molecular pathology, and biomarkers. Neurology. 2007;68:812–9. https://doi.org/10.1212/01.wnl.0000256715.13907.d3

7. McKeith IG, Dickson DW, Lowe J, Emre M, O'Brien JT, Feldman H, et al.; Consortium on DLB. Diagnosis and management of dementia with Lewy bodies: third report of the DLB Consortium. Neurology. 2005;65:1863–72. https://doi.org/10.1212/01.wnl.0000187889.17253.b1

8. Förstl H, Burns A, Luthert P, Cairns N, Levy R. The Lewy-body variant of Alzheimer's disease. Clinical and pathological findings. Br J Psychiatry. 1993;162:385–92. https://doi.org/10.1192/bjp.162.3.385

9. Hamilton RL. Lewy bodies in Alzheimer's disease: a neuropathological review of 145 cases using alpha-synuclein immunohistochemistry. Brain Pathol. 2000;10:378–84.

10. Raghavan R, Khin-Nu C, Brown A, Irving D, Ince PG, Day K, et al. Detection of Lewy bodies in trisomy 21 (Down's syndrome). Can J Neurol Sci. 1993;20:48–51. https://doi.org/10.1017/S0317167100047405

11. Galpern WR, Lang AE. Interface between tauopathies and synucleinopathies: a tale of two proteins. Ann Neurol. 2006;59:449–58. https://doi.org/10.1002/ana.20819

12. Mattila PM, Röyttä M, Torikka H, Dickson DW, Rinne JO. Cortical Lewy bodies and Alzheimer-type changes in patients with Parkinson's disease. Acta Neuropathol. 1998;95:576–82. https://doi.org/10.1007/s004010050843

13. Jensen PH, Hojrup P, Hager H, Nielsen MS, Jacobsen L, Olesen OF, et al. Binding of Abeta to alpha- and beta-synucleins: identification of segments in alpha-synuclein/NAC precursor that bind Abeta and NAC. Biochem J. 1997;323(Pt 2):539–46. https://doi.org/10.1042/bj3230539

14. Jensen PH, Sørensen ES, Petersen TE, Gliemann J, Rasmussen LK. Residues in the synuclein consensus motif of the alpha-synuclein fragment, NAC, participate in transglutaminase-catalysed cross-linking to Alzheimer-disease amyloid beta A4 peptide. Biochem J. 1995;310(Pt 1):91–4.

15. Mandal PK, Pettegrew JW, Masliah E, Hamilton RL, Mandal R. Interaction between Abeta peptide and alpha synuclein: molecular mechanisms in overlapping pathology of Alzheimer's and Parkinson's in dementia with Lewy body disease. Neurochem Res. 2006;31:1153–62. https://doi.org/10.1007/s11064-006-9140-9

16. Tsigelny IF, Crews L, Desplats P, Shaked GM, Sharikov Y, Mizuno H, et al. Mechanisms of hybrid oligomer formation in the pathogenesis of combined Alzheimer's and Parkinson's diseases. PLoS One. 2008;3:e3135. https://doi.org/10.1371/journal.pone.0003135

17. Wirths O, Weickert S, Majtenyi K, Havas L, Kahle PJ, Okochi M, et al. Lewy body variant of Alzheimer's disease: alpha-synuclein in dystrophic neurites of A beta plaques. NeuroReport. 2000;11:3737–41. https://doi.org/10.1097/00001756-200011270-00029

18. Outeiro TF, Koss DJ, Erskine D, Walker L, Kurzawa-Akanbi M, Burn D, et al. Dementia with Lewy bodies: an update and outlook. Mol Neurodegener. 2019;14:5. https://doi.org/10.1186/s13024-019-0306-8

19. Thomas AJ, Mahin-Babaei F, Saidi M, Lett D, Taylor JP, Walker L, et al. Improving the identification of dementia with Lewy bodies in the context of an Alzheimer's-type dementia. Alzheimers Res Ther. 2018;10:27. https://doi.org/10.1186/s13195-018-0356-0

20. Attems J, Walker L, Jellinger KA. Olfactory bulb involvement in neurodegenerative diseases. Acta Neuropathol. 2014;127:459–75. https://doi.org/10.1007/s00401-014-1261-7

21. Barresi M, Ciurleo R, Giacoppo S, Foti Cuzzola V, Celi D, Bramanti P, et al. Evaluation of olfactory dysfunction in neurodegenerative diseases. J Neurol Sci. 2012;323:16–24. https://doi.org/10.1016/j.jns.2012.08.028

22. Bachhuber T, Katzmarski N, McCarter JF, Loreth D, Tahirovic S, Kamp F, et al. Inhibition of amyloid-β plaque formation by α-synuclein. Nat Med. 2015;21:802–7. https://doi.org/10.1038/nm.3885

23. Wesson DW, Wilson DA, Nixon RA. Should olfactory dysfunction be used as a biomarker of Alzheimer's disease? Expert Rev Neurother. 2010;10:633–5. https://doi.org/10.1586/ern.10.33

24. Wu N, Rao X, Gao Y, Wang J, Xu F. Amyloid-β deposition and olfactory dysfunction in an Alzheimer's disease model. J Alzheimers Dis. 2013;37:699–712. https://doi.org/10.3233/JAD-122443

25. Heyman A, Fillenbaum GG, Gearing M, Mirra SS, Welsh-Bohmer KA, Peterson B, et al. Comparison of Lewy body variant of Alzheimer's disease with pure Alzheimer's disease: consortium to establish a registry for Alzheimer's Disease, Part XIX. Neurology. 1999;52:1839–44.

26. Kallhoff V, Peethumnongsin E, Zheng H. Lack of alpha-synuclein increases amyloid plaque accumulation in a transgenic mouse model of Alzheimer's disease. Mol Neurodegener. 2007;2:6. https://doi.org/10.1186/1750-1326-2-6

27. Radde R, Bolmont T, Kaeser SA, Coomaraswamy J, Lindau D, Stoltze L, et al. Abeta42-driven cerebral amyloidosis in transgenic mice reveals early and robust pathology. EMBO Rep. 2006;7:940–6. https://doi.org/10.1038/sj.embor.7400784

28. Kahle PJ, Neumann M, Ozmen L, Muller V, Jacobsen H, Schindzielorz A, et al. Subcellular localization of wild-type and Parkinson's disease-associated mutant alpha-synuclein in human and transgenic mouse brain. J Neurosci. 2000;20:6365–73.

29. Yang M, Crawley JN. Simple behavioral assessment of mouse olfaction. Curr Protoc Neurosci. 2009;Chapter 8:Unit 8.24. https://doi.org/10.1002/0471142301.ns0824s48

30. Takahashi H, Ogawa Y, Yoshihara S-I, Asahina R, Kinoshita M, Kitano T, et al. A subtype of olfactory bulb interneurons is required for odor detection and discrimination behaviors. J Neurosci. 2016;36:8210–27. https://doi.org/10.1523/JNEUROSCI.2783-15.2016

31. Franklin K, Paxinos G. Paxinos and Franklin's the mouse brain in stereotaxic coordinates. 5th ed. Academic Press. 2019.

32. Steiner H, Kostka M, Romig H, Basset G, Pesold B, Hardy J, et al. Glycine 384 is required for presenilin-1 function and is conserved in bacterial polytopic aspartyl proteases. Nat Cell Biol. 2000;2:848–51. https://doi.org/10.1038/35041097

33. Ziegler-Waldkirch S, d'Errico P, Sauer J-F, Erny D, Savanthrapadian S, Loreth D, et al. Seed-induced Aβ deposition is modulated by microglia under environmental enrichment in a mouse model of Alzheimer's disease. EMBO J. 2018;37:167–82. https://doi.org/10.15252/embj.201797021

34. Katzmarski N, Ziegler-Waldkirch S, Scheffler N, Witt C, Abou-Ajram C, Nuscher B, et al. Aβ oligomers trigger and accelerate Aβ seeding. Brain Pathol. 2020;30:36–45. https://doi.org/10.1111/bpa.12734

35. Meyer-Luehmann M, Coomaraswamy J, Bolmont T, Kaeser S, Schaefer C, Kilger E, et al. Exogenous induction of cerebral beta-amyloidogenesis is governed by agent and host. Science. 2006;313:1781–4. https://doi.org/10.1126/science.1131864

36. Friesen M, Meyer-Luehmann M. Aβ seeding as a tool to study cerebral amyloidosis and associated pathology. Front Mol Neurosci. 2019;12:233. https://doi.org/10.3389/fnmol.2019.00233

37. Meyer-Luehmann M, Stalder M, Herzig MC, Kaeser SA, Kohler E, Pfeifer M, et al. Extracellular amyloid formation and associated pathology in neural grafts. Nat Neurosci. 2003;6:370–7. https://doi.org/10.1038/nn1022

38. Torres M, Jimenez S, Sanchez-Varo R, Navarro V, Trujillo-Estrada L, Sanchez-Mejias E, et al. Defective lysosomal proteolysis and axonal transport are early pathogenic events that worsen with age leading to increased APP metabolism and synaptic Abeta in transgenic APP/PS1 hippocampus. Mol Neurodegener. 2012;7:59. https://doi.org/10.1186/1750-1326-7-59

39. Knowles TPJ, Waudby CA, Devlin GL, Cohen SIA, Aguzzi A, Vendruscolo M, et al. An analytical solution to the kinetics of breakable filament assembly. Science. 2009;326:1533–7. https://doi.org/10.1126/science.1178250

40. Sharma SK, Chorell E, Steneberg P, Vernersson-Lindahl E, Edlund H, Wittung-Stafshede P. Insulin-degrading enzyme prevents α-synuclein fibril formation in a nonproteolytical manner. Sci Rep. 2015;5:12531. https://doi.org/10.1038/srep12531

41. Sharma SK, Chorell E, Wittung-Stafshede P. Insulin-degrading enzyme is activated by the C-terminus of α-synuclein. Biochem Biophys Res Commun. 2015;466:192–5. https://doi.org/10.1016/j.bbrc.2015.09.002

42. Derecki NC, Katzmarski N, Kipnis J, Meyer-Luehmann M. Microglia as a critical player in both developmental and late-life CNS pathologies. Acta Neuropathol. 2014;128:333–45. https://doi.org/10.1007/s00401-014-1321-z

43. Mandrekar S, Jiang Q, Lee CYD, Koenigsknecht-Talboo J, Holtzman DM, Landreth GE. Microglia mediate the clearance of soluble Abeta through fluid phase macropinocytosis. J Neurosci. 2009;29:4252–62. https://doi.org/10.1523/JNEUROSCI.5572-08.2009

44. Parhizkar S, Arzberger T, Brendel M, Kleinberger G, Deussing M, Focke C, et al. Loss of TREM2 function increases amyloid seeding but reduces plaque-associated ApoE. Nat Neurosci. 2019;22:191–204. https://doi.org/10.1038/s41593-018-0296-9

45. Sarlus H, Heneka MT. Microglia in Alzheimer's disease. J Clin Invest. 2017;127:3240–9. https://doi.org/10.1172/JCI90606

46. Brück D, Wenning GK, Stefanova N, Fellner L. Glia and alpha-synuclein in neurodegeneration: a complex interaction. Neurobiol Dis. 2016;85:262–74. https://doi.org/10.1016/j.nbd.2015.03.003

47. Lee E-J, Woo M-S, Moon P-G, Baek M-C, Choi I-Y, Kim W-K, et al. Alpha-synuclein activates microglia by inducing the expressions of matrix metalloproteinases and the subsequent activation of protease-activated receptor-1. J Immunol. 2010;185:615–23. https://doi.org/10.4049/jimmunol.0903480

48. Zhang W, Wang T, Pei Z, Miller DS, Wu X, Block ML, et al. Aggregated alpha-synuclein activates microglia: a process leading to disease progression in Parkinson's disease. FASEB J. 2005;19:533–42. https://doi.org/10.1096/fj.04-2751com

49. Mentlein R, Ludwig R, Martensen I. Proteolytic degradation of Alzheimer's disease amyloid beta-peptide by a metalloproteinase from microglia cells. J Neurochem. 1998;70:721–6. https://doi.org/10.1046/j.1471-4159.1998.70020721.x

50. Alvarado-Martínez R, Salgado-Puga K, Peña-Ortega F. Amyloid beta inhibits olfactory bulb activity and the ability to smell. PLoS One. 2013;8:e75745. https://doi.org/10.1371/journal.pone.0075745

51. Hernández-Soto R, Rojas-García KD, Peña-Ortega F. Sudden intrabulbar amyloid increase simultaneously disrupts olfactory bulb oscillations and odor detection. Neural Plast. 2019;2019:3424906. https://doi.org/10.1155/2019/3424906

## SUPPORTING INFORMATION

Additional supporting information may be found in the online version of the article at the publisher's website.

**TABLE S1** Number of mice analyzed

**TABLE S2** Number of seeded and grafted mice used and analyzed

**FIGURE S1** (A) Immunofluorescent staining of Aβ plaques (6E10, green and DAPI, blue) and compact Aβ plaque load (Thiazine red (TR), red and DAPI, blue) in olfactory bulbs of 12-month-old male *APPPS1, APPPS1 x [A30P]aSYN* and *WT* animals. Scale bar represents 200 μm. (B) Assessment of total Aβ load based on 6E10 immunostaining and (C) of compact $TR^+$ Aβ deposits. Each symbol represents data from one mouse (*APPPS1*: $n = 8$, *APPPS1 x [A30P]aSYN*: $n = 7$). Data are presented as mean ± SEM. (D) Enzyme-linked immunosorbent assays (ELISA) for soluble and insoluble $Aβ_{40}$ and (E) soluble and insoluble $Aβ_{42}$ peptide fractions of olfactory bulb brain extracts from 12-month-old *APPPS1* and *APPPS1 x [A30P]aSYN* mice. Each symbol represents data from one mouse (*APPPS1*: $n = 5$-$6$, *APPPS1 x [A30P]aSYN*: $n = 6$). Data were normalized to *APPPS1*. Data are presented as mean ± SEM. (F) Representative immunoblots of olfactory bulb brain extracts from 12-month-old male *APPPS1* and *APPPS1 x [A30P]aSYN* mice. Immunoblots were probed with antibodies that recognize full-length APP, CTFβ and CTFα (6687) and Aβ (6E10). β-Actin was used as loading control

**FIGURE S2** (A) Representative images of immunofluoresent staining of Reelin (red) cells from 8-month-old *APPPS1* and *APPPS1 x [A30P]aSYN* mice. Nuclei were counterstained with DAPI (blue). Scale bar represents 200 μm. (B) Quantification of $Reelin^+$ cells in the mitral cell layer. Each symbol represents data from one mouse (*APPPS1*: $n = 5$, *APPPS1 x [A30P]aSYN*: $n = 5$). Data are presented as mean ± SEM. (C) Representative images of Neurotrace (green) staining of 8-month-old *APPPS1* and *APPPS1 x [A30P]aSYN* mice. Nuclei were counterstained with DAPI (blue). Scale bar represents 200 μm. (D) Assessment of Neurotrace-positive cells in the mitral cell layer. Each symbol represents data from one mouse (*APPPS1*: $n = 5$, *APPPS1 x [A30P]aSYN*: $n = 5$). Data are presented as mean ± SEM